

# Assessment of Effect of Flux Scheme and Turbulence Model on Blade-to-blade Calculations

M. Bilgiç<sup>1†</sup>, Ö. U. Baran<sup>1</sup> and M. H. Aksel<sup>2</sup>

<sup>1</sup> *Department of Mechanical Engineering, Middle East Technical University, Ankara, Çankaya, 06800, Turkey*

<sup>2</sup> *Department of Aeronautical Engineering, University of Turkish Aeronautical Association, Ankara, Etimesgut, 06790, Turkey*

†Corresponding Author Email: [mustafa.bilgic@tei.com.tr](mailto:mustafa.bilgic@tei.com.tr)

## ABSTRACT

Today, due to advances in computing power, Reynolds Averaged Navier-Stokes (RANS) solvers are widely preferred for quasi-three-dimensional (Q3D) blade-to-blade analysis. This study investigates the performance of different flux calculation methods and turbulence models with a density-based RANS solver (Numeca®) in blade-to-blade analysis. A block-structured mesh topology is used to create a solution grid around the airfoil. Spatial discretization is performed in the pitchwise direction to represent the quasi three-dimensional flow, while only one computational cell is used in the radial direction to simulate the flow through the Q3D cascade. The computational grid around the airfoil is created with the Autogrid® tool using the block mesh topology. For the convective flow calculations, both the central and upwind methods available in Numeca® are applied separately. The Baldwin Lomax (BL), Spalart Allmaras (SA), Shear Stress Transport (SST), Explicit Algebraic Reynolds Stress Model (EARSM) and  $k-\epsilon$  (KEPS) turbulence models are used for the turbulent shear stress calculations. In order to evaluate the aerodynamic performance of the spatial discretization methods and turbulence models, the isentropic Mach distribution on the airfoil surface, the total pressure loss and the exit flow angle behind the blade are compared with the experimental data of six test cases. In the compressor cases, the Spalart-Allmaras turbulence model with the Central scheme gives the best results in terms of average loss prediction, while no turbulence model is superior to the other in terms of exit angle prediction. On the turbine side, EARSM and KEPS give better performance in terms of loss prediction for the low Reynolds case compared to others, while the Spalart-Allmaras turbulence model is better for the high Reynolds cases.

## Article History

Received August 17, 2023

Revised January 16, 2024

Accepted February 4, 2024

Available online April 30, 2024

## Keywords:

*Blade to Blade  
Turbulence Model  
Upwind  
Central  
Shock Wave  
Boundary Layer*

## 1. INTRODUCTION

The axial turbomachinery design process begins with mean line analysis. In this phase of the design, the initial dimensions of the flow path and the blades are determined. After the complete flow quantities are determined at the mean radius, the successive solution of the flow equations on the throughflow ( $r-z$  plane) and blade-to-blade ( $m-\theta$ ) planes is required to define the complete three-dimensional flow field (Wu, 1952). The distribution of kinematic and thermodynamic quantities along the blade span in the meridional plane is determined by the flow analysis. Since the meridional analysis cannot predict the pitchwise variation of the flow quantities, the loss and deviation angles must be given externally. There are two ways to calculate loss and deviation in meridional analysis. The first way is to use correlations obtained from

experimental data. This may be the best way to start a two-dimensional design, but correlations may not be sufficient to capture the effects of some physical phenomena such as shock wave and separation. The blade-to-blade solver plays an important role at this stage of the design process. Since the flow equations are solved in the  $m-\theta$  plane, all the details of the flow field can be captured. Therefore, the second and more reliable way to calculate loss and deviation is the blade-to-blade solution. In addition to calculating the loss and deviation, the aerodynamic loading of the blade profile is determined by blade-to-blade calculations. The location of the shock wave, the diffusion factor, the aerodynamic load on the blade profile (lift force), and the optimum angle of incidence are also determined by the blade-to-blade calculations.

The boundary layer, shock and trailing edge losses are the loss mechanisms that can be calculated by the blade to

Nomenclature		Subscripts / Superscripts	
<b>symbols</b>		1	state belongs to inlet plane
$\varphi$	$\tan^{-1}(V_r/V_m)$	2	state belongs to exit plane
$\beta$	$\tan^{-1}(V_t/V_m)$	is	isentropic
$V_r$	radial velocity	<b>Abbreviations</b>	
$V_t$	tangential velocity	RANS	Reynolds Averaged Navier Stokes
$V_m$	meridional velocity	Q3D	quasi three dimensional
$V$	absolute velocity	SA	Spalart Allmaras
$\omega = \frac{P_{01}-P_{02}}{P_{01}-P_{s1}}$	total pressure loss coefficient for compressor cascades	BL	Baldwin Lomax
$Y = \frac{P_{01}-P_{02}}{P_{02}-P_{s2}}$	total pressure loss coefficient for turbine cascades	SST	Shear Stress Transport
$\zeta = 1 - \frac{V_z^2}{V_{zis}^2}$	enthalpy loss coefficient for turbine cascades	EARSM	Explicit Algebraic Reynolds Stress Model
$\eta$	pitchwise direction	KEPS	k – $\epsilon$ turbulence model
$t$	cascade pitch	CENT	Central Spatial Discretization Scheme
		UPW	Upwind Discretization Scheme

blade analysis. The boundary layer loss is directly proportional to the momentum thickness and the shape factor. The momentum thickness is a function of the streamwise pressure gradient and the frictional force near the wall. In a decelerating flow, the contribution of the streamwise pressure gradient becomes dominant compared to the contribution of the frictional force (Braembussche 2005). When the flow is transonic, the shock loss occurs in addition to the boundary layer loss. Boundary layer separation can occur depending on the strength of the shock wave. Trailing edge losses are the last type of loss mechanism that can be treated by blade to blade analysis. The high-speed jet flow is mixed with the wake formed by the finite thickness of the trailing edge. The mixing process introduces additional boundary layer losses and shock losses. The trailing edge loss components are the dominant mechanism for the turbines due to the thick trailing edge. The effect of trailing edge loss increases when a shock wave is formed at the trailing edge.

There are several methods in the literature for solving blade-to-blade flow. The method of Wu (1952) is a good approximate solution, but it was insufficient for transonic flow calculations. The transonic principal equation is of elliptic type in the subsonic region and of hyperbolic type in the supersonic region. Since the principal equation has different characteristics for subsonic and supersonic flow, it can only handle subsonic flow or only supersonic flow. This is actually the general problem of the steady-state solvers. To overcome this difficulty, the first transonic potential equation was introduced by Murman and Cole (1971). They introduced numerical viscosity in the supersonic regime. This method can capture the shock without any loss of mass flux, but the momentum is not conserved due to the nature of the potential flow. The Newton method is applied to the Euler and Navier-Stokes equations by Childs and Pulliam (1984). The Newton method worked, but it does not have any advantages over the traditional time marching methods in terms of accuracy and speed. An early method used to compute the steady-state. Giles (1985) has combined the streamline grids of the streamline curvature method and the conservative formulation of the finite volume method. The

steady-state integral form of the Euler equations is applied to the quadrilateral cells. To cover the transonic flow, the artificial compressibility concept has been implemented by Giles (1985) similar to the application of Murman and Cole (1971). So far, all solution algorithms require boundary layer correction because they are inviscid solvers. Therefore, the early blade-to-blade solvers predict the losses poorly because only the boundary layer losses can be considered.

The latest and most advanced solution method is the time marching The Reynolds Averaged Navier Stokes (RANS) solver. Since the characteristic of the Euler part of the RANS equation is of hyperbolic type for all flow regimes (subsonic, transonic, supersonic), transonic flow can be solved without any additional treatment such as artificial compressibility. RANS solvers have the ability to capture all of the loss mechanisms mentioned above. The unsteady form of the RANS equations is parabolic in time, which means that transonic flow can be handled without any numerical problems. Since the RANS equations include the shear stress terms, the boundary layer can be resolved quite accurately if a suitable boundary layer grid is generated near the wall. In the early days, time-domain solution techniques were not preferred due to lack of computing power. However, today, even simple personal computers can solve the RANS equation on a blade-to-blade surface in a few seconds.

In this study, the capabilities of the RANS solver are tested for different turbulence models and flux schemes. Three compressor and three turbine experimental test cases are selected to compare the numerical results. The commercial tool Numeca® is selected as the flow solver. The central scheme (CENT) with artificial dissipation and upwind (UPW) schemes are available for inviscid flux calculation in it. Among the turbulence models, Spalart Allmaras (SA), Baldwin Lomax (BL), k-epsilon (KEPS), shear stress transport (SST) and Explicit Algebraic Reynolds Stress Model (EARSM) models are selected for the calculation of turbulence stresses. The results are compared with experimental data in terms of isentropic Mach number at the blade surface, loss generated behind the blade row, and exit flow angles.

**Table 1 Main Characteristics of Test Cases**

	$M_{in}$	$Re_{in}$ ( $\times 10^6$ )	c/s	Static Pressure Ratio	AVDR
1	0.800	0.500	0.450	1.30	1.20
2	1.086	1.500	0.621	1.45	1.18
3	1.616	1.132	0.654	1.88	1.10
	$M_{ex}$	$Re_{ex}$ ( $\times 10^6$ )	s/c	Stagger Angle	AVDR
4	0.71	0.29	0.564	19.60	0.91
5	1.02	1.00	0.850	55.00	1.00
6	1.00	0.76	0.710	33.30	0.92

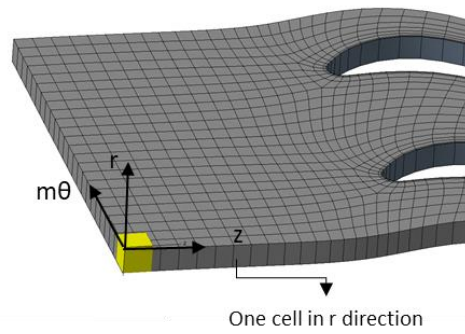


**Fig. 1 One cell mesh structure for cascade analysis**

**2. DEFINITION OF THE TEST CASES**

In order to investigate all possible physical phenomena in cascade flow, both subsonic and transonic cases are selected for compressor and turbine. The first test case is a high-turning (50 degrees) compressor cascade with an inlet Mach number of 0.8 (Hoheisel & Seyb 1990). The second case is the low supersonic compressor cascade with an inlet Mach number of 1.086 and 13 degrees of flow turning (Starken & Schreiber, 1990). The oblique shock wave occurs on the suction side of the blade. The third case is the high supersonic compressor cascade with very low flow turning (about 1 degree) and an inlet Mach number of 1.61 (Starken & Schreiber, 1990). The oblique shock is formed in front of the leading edge and normal shocks appear after the throat. The boundary layer is also significantly affected due to the formation of strong shock waves.

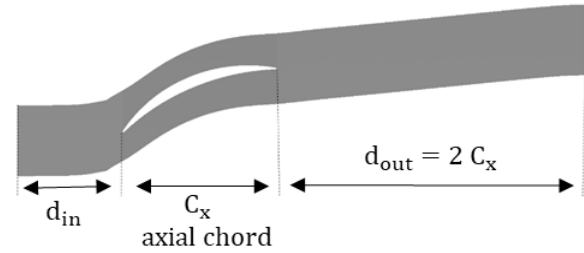


**Fig. 2 Computational domain for the cascade analysis**

The next three cases are the turbine cascades. The first one is a high speed low pressure turbine (LPT) rotor blade (Denton et al., 1990). The exit Reynolds number is set to  $2.9 \times 10^5$  to simulate low Reynolds flow conditions. The flow separates and re-attaches at the location with 80% axial chord distance from the leading edge on the suction surface. The next case is the well-known VKI LS 89 (Von Karman Institute lecture series 89) transonic NGV case (Arts et al., 1990). This is the challenging test case due to high acceleration and flow deflection. The final test case is the VKI LS 59 transonic cascade (Kiock et al., 1986). It is a representative test case for the transonic rotor blades. The main characteristics of all test cases are summarized in Table 1.

**3. NUMERICAL SETUP**

Since the two-dimensional analysis mode is not available in NUMECA, the one-cell approach is used to simulate cascade analysis. The one-cell approach allows for a quasi-three-dimensional calculation using a three-dimensional computational domain. When a block-structured mesh is assigned to the blade-to-blade plane ( $z$ - $m\theta$  plane in Fig. 1), a single cell is used in the radial direction ( $r$  direction in Fig. 1) to represent the flow through the stream tube. The computational domain shown in Fig. 2 is used for all cascade test cases. The distance between the inlet boundary and the leading edge of the blade is determined according to the measurement plane defined in the experimental setup.

It is common practice for turbomachinery boundary conditions to impose the total temperature and pressure at the inlet. To fully define the inlet boundary, the velocity field must also be imposed. This can be done by defining either the magnitudes of the velocity components or the angles. In all analyses, the total temperature and pressure at the inlet boundary are imposed. In the high subsonic compressor case and all turbine cases, the flow angles  $\varphi$  and  $\beta$  to the inlet boundary are given. In the low and high supersonic compressor cases, the tangential velocity component "Vt" is imposed instead of the  $\beta$ . At the outlet boundary, only the average static pressure is imposed. The upper and lower surfaces in the  $r$ -direction are treated as an Euler wall (slip boundary) so that the two-dimensional nature of the flow through the cascade can be represented. The periodic boundary conditions are applied to the literal surfaces. Turbulence quantities are defined according to the experimental setup. The mass flow balance between the inlet and outlet planes and the mixed out loss coefficients are used as convergence check parameters for all analyses, as with all CFD analyses. Because the mass flow rate converges faster than the loss coefficient, a CFD run is not terminated until the total pressure loss value has reached its steady-state value. The finite volume method with explicit time integration is used to solve the unsteady RANS equations. This study evaluates two well-known inviscid flow calculation methods, the central and the upwind schemes, focusing on the compressible flow within the blade to the blade surface. Both schemes are available in Numeca®. In addition to the turbulence models mentioned above, appropriate transition models in Numeca® are activated for all test cases.

Figure 3 shows a detailed example of the mesh generated around the blade. The block structure of the mesh allows it to surround the blade very well in the leading and trailing edge areas. On the suction and pressure sides, a streamlined mesh is generated to capture

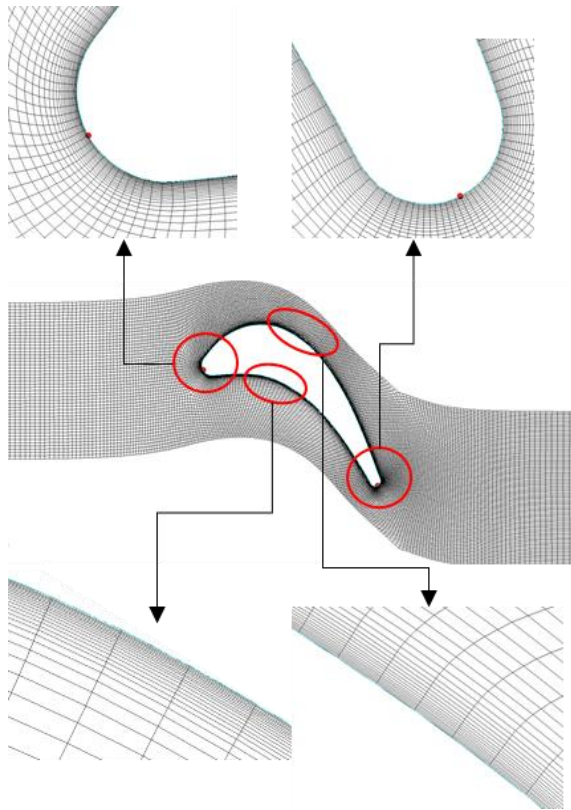


**Fig. 3** Details of the generated mesh around the airfoil

the gradients in the flow direction well, thanks to the block surrounding the blade.

## 4. SIMULATION RESULTS

### 4.1 Subsonic Compressor Cascade

The first test case is a subsonic test case. The experimental test data are presented in (Hoheisel & Seyb 1990) and involve an axial compressor cascade with 50 degrees of turn and an absolute inlet Mach number of 0.8. The Mach number is still high where compressibility effects dominate. There are no shock waves through the channel, but a supersonic pocket appears near the leading edge on the suction side. There is also a thick trailing edge boundary layer which increases the flow deviation from the blade. The Mach number contour is shown in Fig. 4.

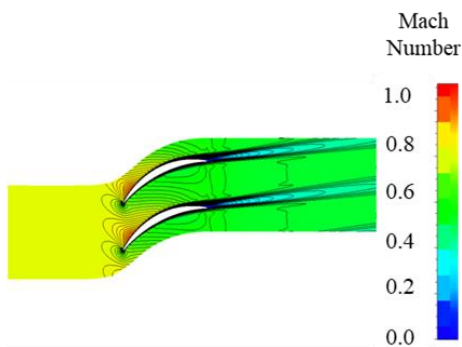


**Fig. 4** Mach contour around the blade, test case 1

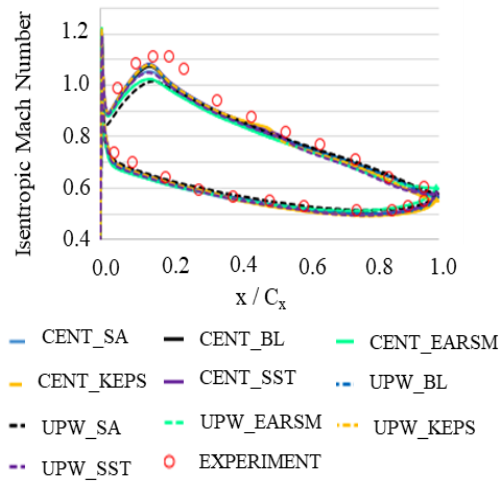


**Fig. 5** Isentropic Mach numbers around the blade, test case 1

The isentropic Mach number distribution around the blade calculated with different solver setups is shown in Fig. 5. It can be seen that modern flow solvers simulate high-subsonic flow in the cascades in a similar way. All methods show a similar deviation from the experimental data. There is no clear distinction between the central and upwind methods. Some turbulence model-flow algorithm combinations perform worse than others. The explicit algebraic Reynolds stress model with the central algorithm deviates the most from the experimental data. The UPW-SA method also deviates from the other solutions on the suction side.

Two factors mainly determine the total pressure drop in this test case. The first is the wall friction and the second is the trailing edge wake. The sum of these losses is integrated into the loss factor. The loss coefficient is calculated for this test case and is listed in Table 2. Experimental data gives a loss of 4.8%, while CFD solutions vary between 3.8% and 7.5%. In general, the selected solver configurations performed well, with the exception of the UPW-EARSM and UPW-SA models.

**Table 2** Result of flow turning and loss coefficient belonging subsonic compressor case

	Method	$ \beta_1 - \beta_2 $ [deg.]	$\omega$
Experiment		48.15	0.0481
Central	BL	48.61	0.0450
	SA	48.29	0.0445
	KEPS	48.21	0.0384
	EARSM	46.40	0.0446
	SST	46.36	0.0381
Upwind	BL	48.76	0.0458
	SA	48.01	0.0753
	KEPS	47.69	0.0555
	EARSM	46.43	0.0513
	SST	46.98	0.0400

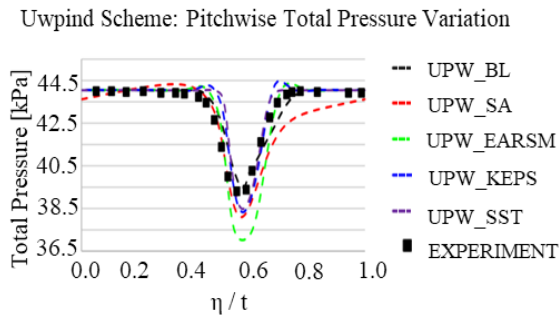
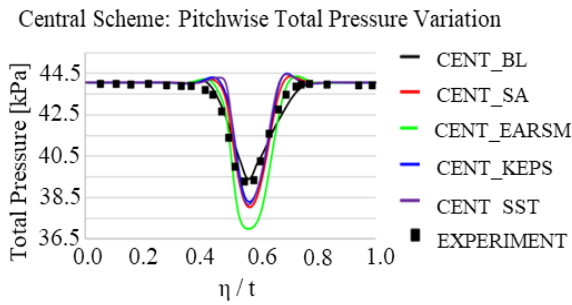


**Fig. 6 Total pressure along the circumferential direction at measuring plane, test case 1**

The other measure is the deviation angle. All of the models are able to calculate the prediction of the angle of turning with a difference of 2 deg. from the experimental data. The BL, SA and KEPS give quite accurate flow turning compared to the experimental data.

The difference between the experimental and numerical results of the loss factor yields interesting results. Figure 6 shows the pitchwise total pressure results at the location of the measurement plane in the experimental setup. This measurement shows the effect of the trailing edge wake zone, which is a significant part of this test case. These plots are divided into central and upwind scheme plots. First, we observe that the wake initiation location is estimated later than the actual location, especially in the central schemes. This results in a narrower low pressure zone. Strangely, the total pressure is increased in front of the wake. This is not physical. Finally, many models overpredict the total pressure loss in the central zone. This behavior compensates for the error in the loss factor calculation in the preprocessing step. In other words, although the wake is not accurately captured, the integration gives good results. The situation improves with upwind methods. The overestimation of the total pressure is largely eliminated, the wake location is slightly improved, and the overestimation at the center is reduced. We observe that EARSM predicts a stronger wake for both central and upwind methods. In fact, it is clear from Fig. 6 why the UPW – SA method gives too much loss. While the total pressure values on the pressure side are perfectly captured, the suction side ( $\eta/t > 0.5$ ) shows a very large total pressure loss from the experiment.

#### 4.2 Low Supersonic Compressor Cascade

The experimental data of the low supersonic compressor cascade are taken from reference (Starken & Schreiber 1990). Unlike the previous one, the test case consists of an apparent shock observed at the suction

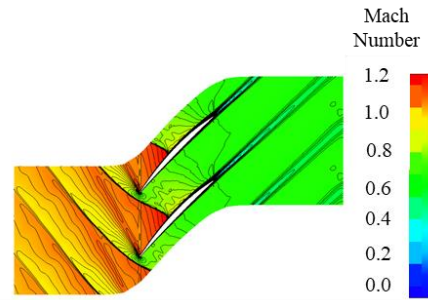


**Fig. 7 Mach contour around the blade, test case 2**

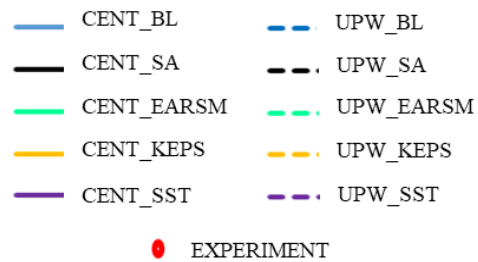
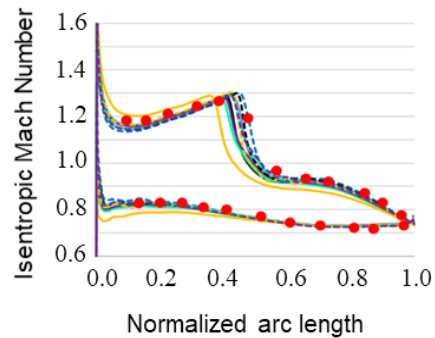


**Fig. 8 Isentropic Mach numbers around the blade, test case 3**

side. The shock visible in the experimental data is located just before the mid section on the suction side. Before discussing the simulation results, we should mention that the 2nd test case is a surprisingly challenging one. The location of the suction-side shock is about to merge with the pressure-side leading edge. The experimental data do not include measuring stations at the leading-edge section. Therefore, we do not know if there is a weak shock at this location or not. Some models start predicting shocks at minimal back pressure changes, while others follow the trend at slightly larger back pressure changes. Therefore, we decided to work with a setup where the shock does not merge into the pressure side. Note that our boundary conditions are fully consistent with the test data. An example run is shown in Fig. 7.

Comparing the numerical results, it is evident that the upwind schemes predict stronger shocks with the same turbulence model, as shown in Fig. 8. A stronger shock does not necessarily imply a better solution, location is also important. We also observe reasonably good results with the central schemes on the suction side. It is observed that the turbulence model has a significant impact on the strength and location of the shock. In general, the SST, KEPS and explicit algebraic Reynolds stress models show similar behavior. The k-ε and k-ω derivative models are

**Table 3 Result of flow turning and loss coefficient belonging low supersonic compressor case**

	Method	$ \beta_1 - \beta_2 $ [deg.]	$\omega$
Experiment		45.20	0.0841
Central	BL	44.95	0.0762
	SA	45.36	0.0802
	KEPS	45.51	0.0942
	EARSM	45.52	0.0796
	SST	45.46	0.0781
Upwind	BL	45.10	0.0748
	SA	45.53	0.0756
	KEPS	45.25	0.0807
	EARSM	45.92	0.0748
	SST	45.39	0.0743

the more dissipative, while the Baldwin-Lomax and Spalart-Almaras models obtain sharper shocks. The upwind methods show better agreement with the experimental data for both shock location and strength.

Of course, integral quantities are more critical than the average flow field. We have compared the calculated loss coefficients with the available experimental data. The results are shown in Table 3. Again, the data is quite close to the experimental data. Comparing the loss coefficient data, both UPW&CENT KEPS predicts higher loss compared to other models. The remaining models with CENT&UPW algorithm predict less loss compared to the experimental data. The deviation between the upwind methods is small and their results are quite consistent. The central algorithm solutions vary more with the choice of turbulence model. The variation of the flow angle obtained from the results of the numerical methods is small, as seen in Table 3. In other words, the flow angles predicted by the numerical methods are very close to each other.

We also observe that upwind methods are more accurate in the simulation of the flow. The striking results are given in Fig. 9. This figure shows the pitch-wise total pressure deviation for central (upper chart) and upwind methods (lower chart). It is seen that central schemes predict increased total pressure before the wake, which is not a physical result. Again, central schemes predict a stronger wake, which compensates for the error in loss coefficient. The solution on both sides of the blade is close to symmetrical, which is also not true. Flow at one side of the blade is subject to a shock; therefore, total pressure losses should be more prominent. The upwind methods show better compliance with the expected behavior. No significant increase in total pressure is observed on the suction side in the results of CENT. The size and strength of the wake are better than the central schemes. On the shock side, the total pressure recovers more quickly than the experimental results, although it is better than the central schemes. The reason for this may be the dissipative behavior of the turbulence models. The entropy generated at the shock is likely to dissipate quickly downstream.

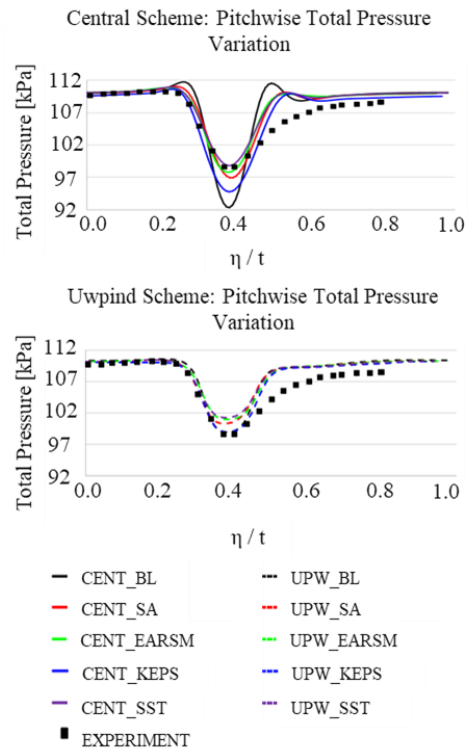


**Fig. 9 Total pressure along the circumferential direction at measuring plane, test case 2**

### 4.3 High Supersonic Compressor Cascade

The third test case consists of a high-supersonic compressor cascade with a very small turning angle of about 1 degree. The inlet Mach number is as high as 1.61 (Starken & Schreiber 1990). These boundary conditions and the blade setup allow for very challenging simulation conditions. The experimental data include many parameters. Therefore, we have the opportunity to compare our results with experimental data for the isentropic Mach number distribution at the blade surface, the exit flow angle distribution, the loss coefficient, and the location of the shock wave. In addition, the calculated flow field can be compared with the schlieren image of the shock wave available in (Starken et al., 1990) and (Tweedt et al., 1988). An example Mach number contour is shown in Fig. 10. The flow field contains almost every complexity. An oblique shock is reflected back inside the flow channel. Shock-Wave Boundary Layer Interaction (SWBLI) effects are visible and the lambda shocks are visible. A normal shock exists at the end of the channel.

The Mach number distribution around the blade is shown in Fig. 11. We observed that the upwind methods have a minimal advantage in shock strength. The main difference around the shocks comes from the turbulence models. Both the suction and pressure side solutions show that the EARSM method tends to give the most smeared results around the shocks. The SST models, on the other hand, preserve the shock strength more sharply. The SA model solutions follow the SST, and both the central and upwind methods yield sharp solutions around the shocks on both sides.

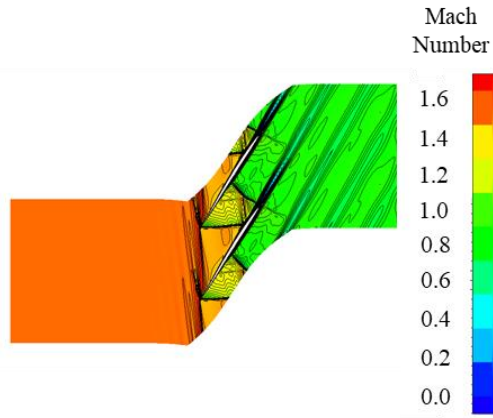


Fig. 10 Mach contour around the blade, test case 3

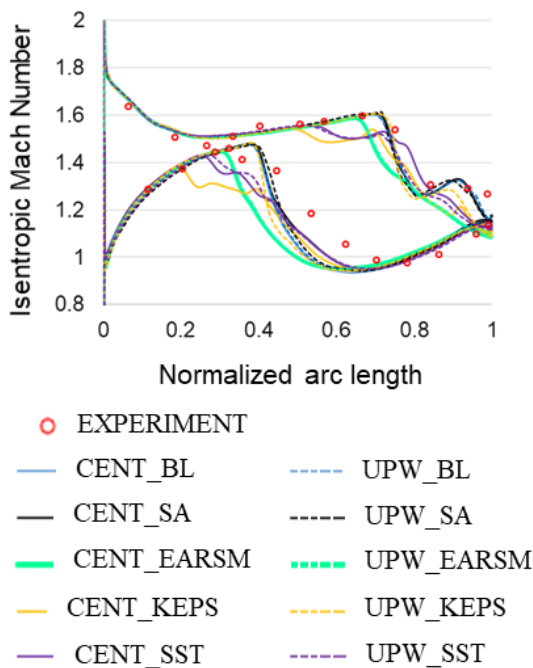


Fig. 11 Isentropic Mach numbers around high supersonic compressor blade, test case 3

Table 4 Result of flow turning and loss coefficient belonging low supersonic compressor case

Method	Method	$ \beta_1 - \beta_2 $ [deg.]	$\omega$
Experiment		59.50	0.1210
Central	BL	57.84	0.1311
	SA	58.66	0.1202
	KEPS	58.70	0.1102
	EARSM	59.01	0.1207
	SST	59.10	0.1111
Upwind	BL	58.32	0.1308
	SA	58.68	0.1188
	KEPS	58.66	0.1232
	EARSM	59.12	0.1196
	SST	58.91	0.1166

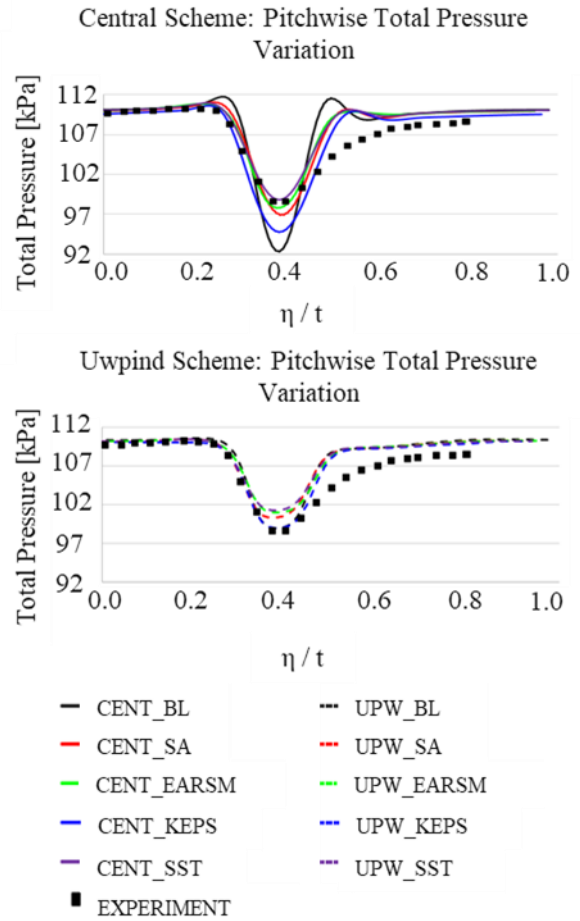


Fig. 12 Total pressure along the circumferential direction at measuring plane for case 3

One of the critical things here is to capture the re-acceleration well after the shock wave. When analyzing the results, both upwind and central results of SA, BL and KEPS models have captured this acceleration. BL and SA results are quite close for both upwind and central schemes. In general, BL gives the closest results to the experiments. However, the detailed analysis of the losses shows that this argument is wrong. The exit flow angle and loss coefficient for case 3 are shown in Table 4 and Fig. 12. Again, the upwind methods give more consistent results. Some central scheme results may seem closer to the experimental data. Curiously, both the central and upwind BL algorithms overpredict the loss coefficient and underpredict the turning angle. This shows us that SWBLI simulation with the BL model deviates from the experimental data. The reason can be at the both extremes. The first reason can be a larger shock allows the shock to penetrate more into the boundary layer region. The second reason is that a late separation results in a larger boundary layer thickness, hence larger mixing losses.

#### 4.4 Low Pressure Turbine Cascade

The first turbine test case is a subsonic turbine cascade with a low exit Reynolds number. The Reynolds number with respect to exit conditions and chord length is set to  $2.9 \cdot 10^5$ . The inlet Mach number of the cascade is 0.5 and it has an isentropic exit Mach number of 0.71. The

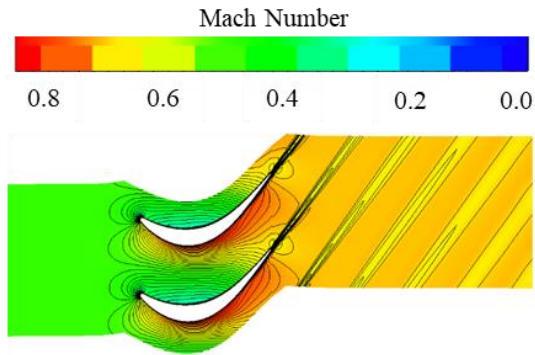
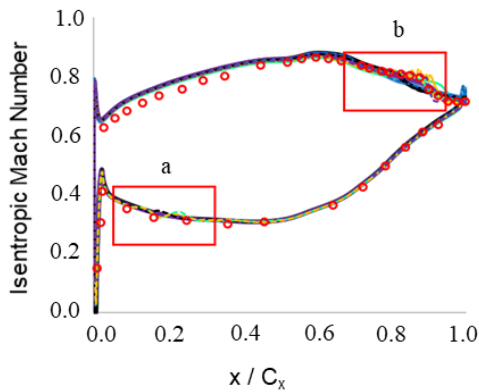


Fig. 13 Mach contour around the blade, test case 4



- EXPERIMENT
- CENT\_BL      - - - - UPW\_BL
- CENT\_SA      - - - - UPW\_SA
- CENT\_EARSM    - - - - UPW\_EARSM
- CENT\_KEPS     - - - - UPW\_KEPS
- CENT\_SST      - - - - UPW\_SST

Fig. 14 Isentropic Mach number around the blade, test case 4

flow is unchoked at the throat, so the flow is completely subsonic within the flow passage. The absolute Mach number around the LPT blade is shown in Fig. 13. The results in terms of isentropic Mach number at the blade surface are shown in Fig. 14. In general, the results look quite similar. However, there is one important point that should be carefully examined. Since this turbine blade operates at a relatively low Reynolds number value, local separation bubbles may occur. The phenomenon mentioned above also occurs in this test case. At about 83 percent of the chord, there is a separation bubble on the suction side (Hodson 1987). There is also another bubble at about 20 percent of the chord (Hodson 1985). The view focusing on this location is shown in Fig. 15. The BL turbulence model with both flux schemes cannot capture any separation at the blade surface. There is a clear difference between the results of the upwind and central schemes. In the case of separation prediction, the central scheme gives poor results. The suction side separation is better predicted by the upwind schemes. The prediction of UPW-KEPS and UPW-EARSM seems to be

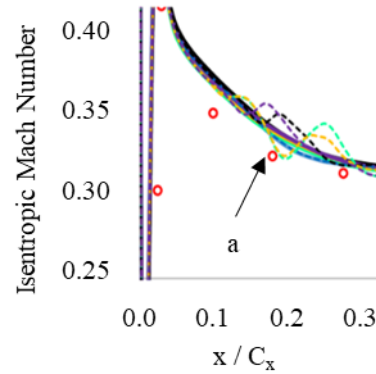
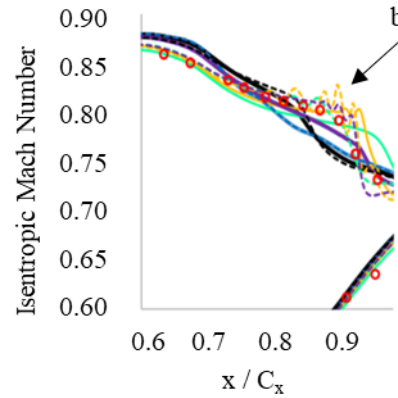


Fig. 15 View that focus on separated region on blade suction and pressure surfaces respectively

Table 5 Result of exit angle and loss coefficient belonging subsonic turbine case

	Method	$\beta_2$ [deg.]	Y
Experiment		53.6	0.0280
Central	BL	53.82	0.0460
	SA	54.01	0.0338
	KEPS	54.36	0.0248
	EARSM	54.46	0.0252
	SST	54.19	0.0248
Upwind	BL	53.82	0.0459
	SA	54.05	0.0341
	KEPS	54.31	0.0279
	EARSM	54.27	0.0278
	SST	54.35	0.0279

more accurate than that of CENT-KEPS and CENT-EARSM. The location of the bubble is accurately captured by the UPW-SST turbulence models. CENT-SST over predicts the size of the separation on the suction side. The SA model with both flow schemes underpredicts the bubble size and captures early separation compared to experimental data. The separation occurring on the pressure side is completely missed by the central schemes with all turbulence models. All turbulence models coupled with upwind schemes predict pressure side separation except the BL turbulence model.

The results showing the deviation angle and loss coefficient are presented in Table 5. The deviation angles

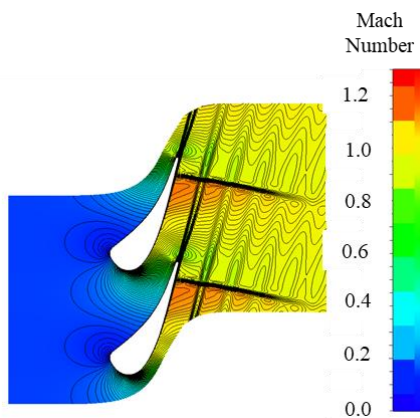


Fig. 16 Mach contour around blade, test case 5

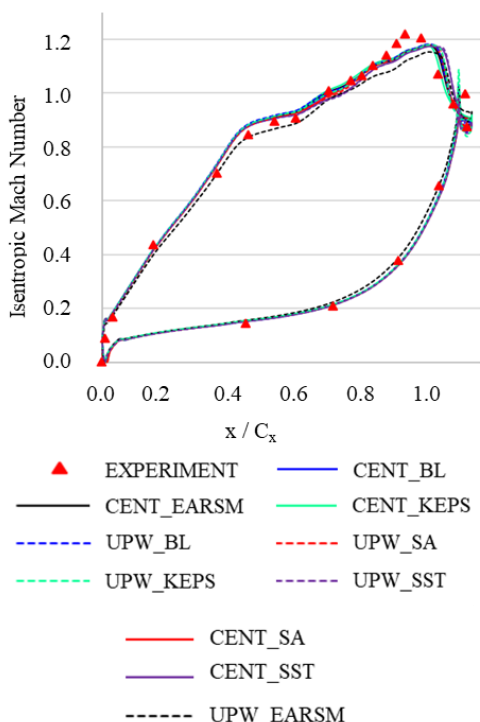


Fig. 17 Isentropic Mach number around the blade, test case 5

obtained from all the analyses are very close to each other. The prediction of the BL turbulence model gives the best result in terms of deviation angle. On the other hand, the worst prediction is given by the BL model in terms of loss coefficient. Regardless of the flow scheme, the SA model also overpredicts the loss coefficient. In terms of loss values, the upwind scheme appears to be more successful compared to the central scheme for the remaining turbulence models. The loss amount obtained from the experiment is almost captured by UPW-KEPS and UPW-SST.

#### 4.5 Transonic Nozzle Guide Vane

The test case is a highly loaded transonic nozzle vane representative of modern engines. The inlet total pressure and temperature are 159.6 kPa and 420 K, respectively. Various conditions are imposed to study the Mach and Reynolds number effects in the report (Arts et al., 1990). In this study, three points were investigated to compare the

Table 6 Result of exit angle and loss coefficient belonging transonic NGV case, Exit Mach=1.02

	Method	$\beta_2$ [deg.]	$\zeta$
Experiment		74.3	0.0272
Central	BL	74.53	0.0363
	SA	74.48	0.0302
	KEPS	74.56	0.0283
	EARSM	74.52	0.0340
	SST	74.53	0.0355
Upwind	BL	74.52	0.0368
	SA	74.49	0.0314
	KEPS	74.56	0.0300
	EARSM	74.52	0.0283
	SST	74.51	0.0349

performance of the numerical methods. The comparison of the numerical methods in terms of surface pressure distribution is made for the MUR 47 condition in the report (Arts et al., 1990). The isentropic Mach number at the exit of the cascade is 1.02. The Mach number contour is shown in Fig. 16.

The isentropic Mach number at the blade surface obtained from each method and experiment is shown in Fig. 17. There is no significant difference between the results. Regardless of the scheme and turbulence model, the shock location is shifted slightly toward the trailing edge compared to the experimental data. Also, the upstream Mach numbers are slightly lower in the numerical results compared to the experiment. The numerical result published in reference (Müller et al., 2018) also gives a similar result to that found in this study. In terms of deviation angle, similar to the results of isentropic Mach number, there are no significant differences between the results of the method. The results in terms of deviation and loss coefficient are presented in Table 6 for the isentropic Mach number of 1.02. However, there are significant differences in the results of the numerical methods in terms of loss coefficient.

Some of the model can give a loss value very close to that of the experiment. However, the loss predictions from numerical simulation are generally higher. In a typical highly loaded turbine, the NGV exit Mach number can be in the interval of 0.85 - 1.1 at the design point. Therefore, the behavior of numerical methods for loss prediction is studied at three points including subcritical, sonic exit and supercritical regimes.

The loss trends obtained from the numerical methods are plotted as a function of the exit isentropic Mach number in Fig. 18. The first experiment is performed by T. Arts at VKI (Arts et al., 1990). The similar study was carried out on the same blade with the same flow conditions (Fontaneto 2014). The results show differences in subcritical region, but very similar to each other after sonic region. At the subsonic side, the loss coefficient is almost flat at the exit isentropic Mach number ranging from 0.7 to 0.95. As the exit Mach number exceeds unity, the shock loss begins to increase and this causes

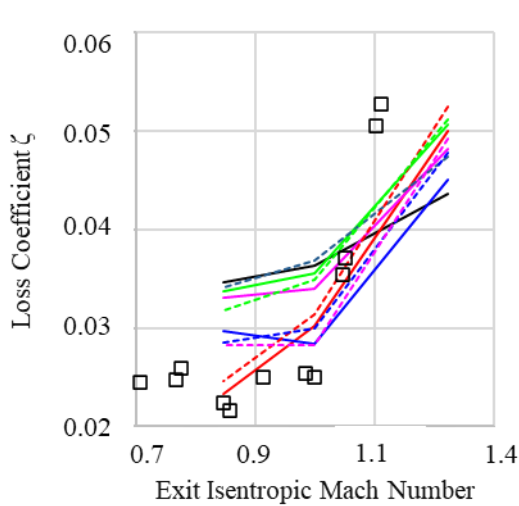


**Fig. 18** Loss coefficient behind the blade as a function of exit isentropic Mach number, test case 5

the loss coefficient to increase. All turbulence models capture the drastic increase after the sonic region, except Baldwin Lomax model. Although their magnitudes are different from each other, the trends look quite compatible with the results of experiments after the sonic point. The loss prediction of KEPS model with both upwind and central scheme gives very good agreement with the experimental data in sonic and supersonic region. Furthermore, the predictions of UPW-SA and UPW-EARSM methods after the sonic region are good in terms of the magnitude of the loss. The differences between the models are obvious in the subsonic region. The experimental data also show different behavior in this region. The loss trends obtained from CENT-KEPS and UPW-EARSM are a little bit different at subsonic exit conditions. In other words, all turbulence models except CENT-KEPS and UPW-EARMS exhibit a decreasing loss trend from exit Mach 1.02 to exit Mach 0.83. Such a result is also seen in [Fontaneto's \(2014\)](#) test results, but the mechanism causing the loss increase in the subsonic range is not fully understood.

#### 4.6 Transonic Turbine Rotor Blade

The test case is a highly loaded, thick transonic rotor blade. The inlet total pressure and temperature are 145 kPa and 278 K, respectively. Various conditions are imposed to study the Mach and Reynolds number effects in the report ([Kiock et al., 1986](#)). Similar to the previous case, only three points including subsonic, sonic and supersonic

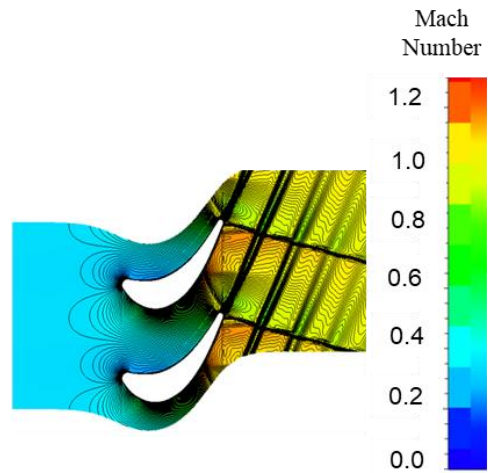


**Fig. 19** Mach contour around blade, test case 6

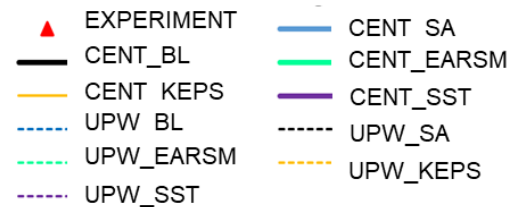
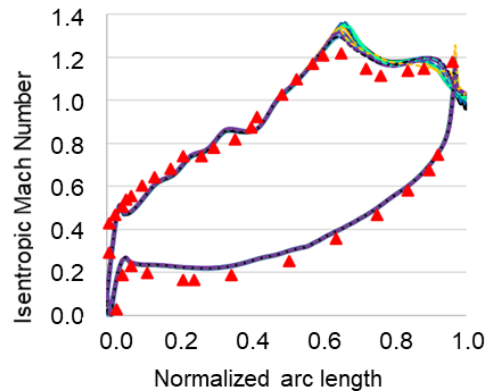


**Fig. 20** Isentropic Mach number on transonic rotor blade

flow were studied to compare the performance of the numerical methods. The Mach number contour around the transonic rotor blade is shown in Fig. 19. The isentropic Mach number distributions are shown in Fig. 20 for an exit Mach number of 0.96. The simulation results are quite similar. The weak shock wave was captured by all numerical methods just after the throat. The shock is slightly shifted towards the trailing edge in the numerical results. This can be easily observed from the isentropic Mach distribution on the blade surface.

The exit angles and loss coefficients at sonic exit conditions are shown in Table 7. The exit angle predictions of the numerical models are very similar to each other. All the numerical results give higher deviation angles compared to the experimental data. In terms of loss coefficient at the sonic condition, the closest loss values

**Table 7 Result of exit angle and loss coefficient belonging transonic rotor case, Exit Mach=1.03**

	Method	$\beta_2$ [deg.]	$\zeta$
Experiment		66.2	0.0551
Central	BL	65.36	0.0380
	SA	65.136	0.0529
	KEPS	65.28	0.0378
	EARSM	65.29	0.0386
	SST	65.2	0.0427
Upwind	BL	65.31	0.0391
	SA	65.11	0.0517
	KEPS	65.21	0.0412
	EARSM	65.23	0.0409
	SST	65.16	0.0440

are obtained from CENT-SA and UPW-SA methods. The remaining simulation results underpredict the total pressure loss. Similar to the previous case, the loss trends are also extracted from the three-point simulation as shown in Fig. 21. In this case, all turbulence models with both upwind and central schemes give good agreement in terms of loss trend. CENT-BL and UPW-BL methods look a little different in the subsonic region. The loss magnitude of CENT-SA and UPW-SA models compromise very well with the experimental data.

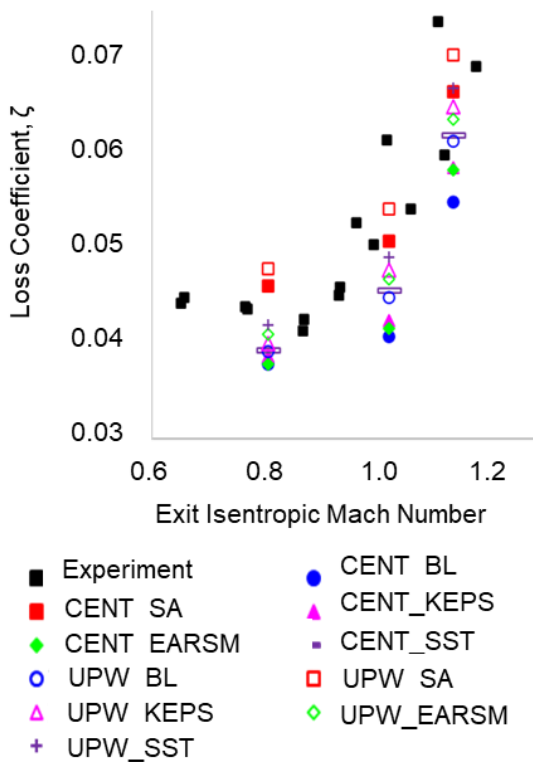


**Fig. 21 Loss coefficient belonging transonic turbine rotor blade as a function of exit isentropic Mach number**

#### 4. CONCLUSION

In this study, the performance of the inviscid flux calculation schemes and turbulence models are investigated. The test cases are selected so that all the flow phenomenon that a designer can face are included. First compressor cases are studied. The upwind scheme with various turbulence model gives more accurate results as compared to central schemes. In general, the deviation angles are more or less are predicted well by the all turbulence model for compressor cases. However, the total pressure predictions show great variation between the models. The best solutions are obtained from SA turbulence model with central scheme in terms of loss prediction in the compressor cases. The upwind SA also gives quite good results except one for case 2. Secondly, the turbine cases are studied. The result of the simulation for the LPT rotor blade has shown that KEPS and EARSM are the best models for low Reynolds flows. SA is the third model, which gives results that are close to those of these two models. In transonic cases, the SA gives best solution in terms of magnitude of loss. However, KEPS and EARSM also give good result in terms of loss trend in transonic region. However, although an analysis of mesh independence has been performed, trailing edge mesh resolution is of critical importance, especially for loss prediction. In this study, the trailing edge mesh resolution is not analyzed in detail, and a change in the mesh structure in this section may change the results obtained in this study. When performing a multi-stage analysis, especially high aspect ratio blades are exposed to less secondary flow and the flow can almost be called Q3D. Therefore, all the results of this study can be applied to the analysis of high aspect ratio turbomachinery.

The following recommendations could be made for the grid settings of B2B analysis as best practices:

1) The number of layers within the boundary layer is of great importance to capture the phenomena such as SWBLI, separation and transition. For the fully turbulent analysis of the transonic compressor and turbine, using more than 33 boundary layer grids within the O grid is sufficient. However, to capture laminar separation and reattachment, more than 49 layers are required within the boundary layer block.

2) For transonic compressors and turbines, the computational domain orientation to accurately capture the shock wave strength and location is of great importance. It is strongly recommended to use a zero-degree from the axial direction periodic boundary upstream of the compressors and downstream of the turbines.

3) A high quality blade-to-blade analysis requires the inclusion of the axial velocity density ratio (AVDR) effect. Especially for the transonic compressors, the AVDR must be strongly applied.

4) On the blade wall, the  $y^+$  values are taken less than 1. This is common practice for CFD applications however it should be noted that very low  $y^+$  values create some convergence problems. Therefore, it is better to use  $y^+$  in the interval of  $0.7 < y^+ < 1.0$ .

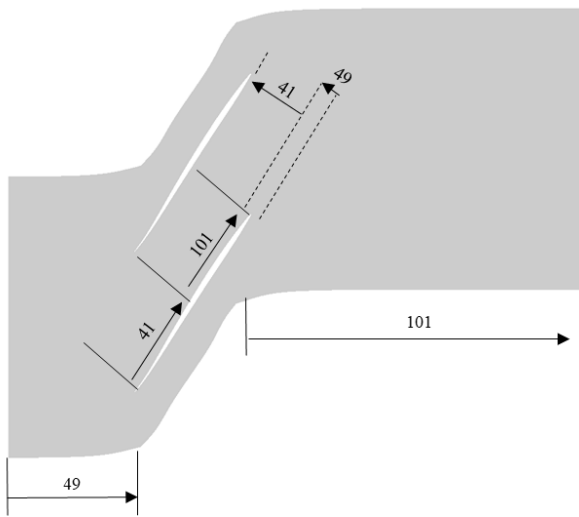


**Fig. 22 Suggested grid number for transonic compressor blade to blade analysis**

5) Note the unique incidence in transonic compressor analysis. When the inlet conditions are supersonic, the inlet angle changes with the inlet Mach number as the correct boundary condition is applied with the Prandtl-Meyer relation. Although modern solvers such as Numeca® do not require very dense mesh structures to capture the shock location and strength, the following mesh settings, which is also sketched in Fig. 22, should be used for proper transonic compressor analysis:

- Upstream streamwise grid number > 49
- Streamwise grid number on the suction surface between the leading edge and throat >41
- Streamwise grid number on the suction surface between throat and trailing edge >101
- The grid number on the normal to streamwise direction excluding boundary layer block (outside the “O” grid block) > 51
- Downstream streamwise grid number > 101

6) In low-pressure turbines, the mesh structure on the unguided section is of great importance in terms of achieving laminar separation. Therefore, the practices obtained from this study, which is also shown in Fig. 23, are as follows:

- Unguided region streamwise grid number > 101
- Capturing the correct boundary layer before the laminar separation is very crucial. Therefore, the streamwise grid point on the suction side between the leading edge and throat > 197
- The grid number on the normal to streamwise direction excluding boundary layer block (outside the “O” grid block) > 81
- Downstream streamwise grid number > 201

7) In high-pressure turbines, the thickening of the boundary layer due to the SWBLI interaction in the unguided region, the accuracy of the shock wave location,

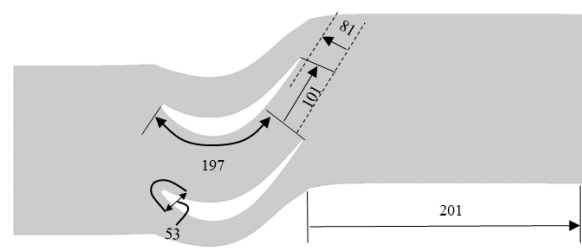


**Fig. 23 Suggested grid number for low pressure turbine blade to blade analysis**

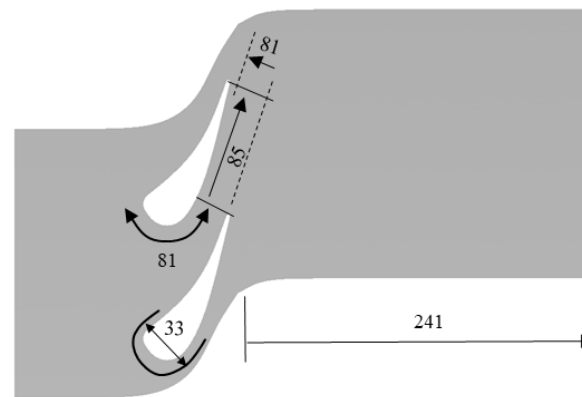


**Fig. 24 Suggested grid number for high pressure turbine blade to blade analysis**

and the shock wave-wake interaction in the downdraft are usually critical. Therefore, the practices obtained from this study, which are also shown in Fig. 24, are as follows:

- Unguided region streamwise grid number > 85
- Capturing the correct boundary layer before the laminar separation is very crucial. Therefore, the streamwise grid point on the suction side between the leading edge and throat > 81
- The grid number on the normal to streamwise direction excluding boundary layer block (outside the “O” grid block) > 81
- Downstream streamwise grid number > 241

### CONFLICT OF INTEREST

All authors declare that they have no conflicts of interest.

### AUTHORS CONTRIBUTION

**Mustafa Bilgiç:** Conceptualization, data curation, investigation, methodology, validation, writing; **Özgür Uğraş Baran:** Supervision, investigation, writing – review & editing; **Mehmet Halûk Aksel:** Supervision, investigation, writing – review & editing

### REFERENCES

Arts, T., & De Rouvoit, M. L. (1990, June 11–14). *Aero-*

- thermal performance of a two dimensional highly loaded transonic turbine nozzle guide vane: a test case for inviscid and viscous flow computations.* Proceedings of the ASME 1990 International Gas Turbine and Aeroengine Congress and Exposition. Volume 1: Turbomachinery. Brussels, Belgium, V001T01A106. ASME. <https://doi.org/10.1115/90-GT-358>
- Braembussche, R. V. (2005). Blade to blade flow in turbomachines. Von Karman Institute for Fluid Dynamics, Course Note 172.
- Childs, R. E., & Pulliam, T. H. (1984, January 9-12). A newton multigrid method for the euler equations. Presented at AIAA 22nd Aerospace Sciences Meeting. <https://doi.org/10.2514/6.1984-430>
- Denton, J. D., Hodson, H. P., & Dominy, R. G. (1990, July). *Tests cases for computation of internal flows in aero engine components test case E/CA-7 subsonic turbine cascade LA.* In AGARD Report No. 275 (AGARD-AR-275).
- Fontaneto, F. (2014). *Aero-thermal performance of a film-cooled high pressure turbine blade/vane: a test case for numerical codes validation* [PhD Thesis, Universita Degli Studi Di Bergamo].
- Giles, M. B. (1985). *Newton solution of steady two-dimensional transonic flow* [PhD Thesis, Department of Aeronautics and Astronautics]. Massachusetts Institute of Technology.
- Hodson, H. P. (1985). Boundary-layer transition and separation near the leading edge of a high-speed turbine blade. *ASME Journal of Engineering for Gas Turbines and Power*, 107(1), 127–134. <https://doi.org/10.1115/1.3239672>
- Hodson, H. P., & Dominy, R. G. (1987). Three-dimensional flow in a low-pressure turbine cascade at its design condition. *ASME Journal of Turbomachinery*, 109(2), 177–185. <https://doi.org/10.1115/1.3262083>
- Hoheisel, H., & Seyb, N. J. (1990). *Tests cases for computation of internal flows in aero engine components test case E/CA-2 high subsonic compressor cascade DCA.* AGARD-AR-275.
- Kiock, R., Lehthaus, F., Baines, N. C., & Sieverding, C. H. (1986). The transonic flow through a plane turbine cascade as measured in four european wind tunnels. *ASME Journal of Engineering for Gas Turbines and Power*, 108(2), 277–284. <https://doi.org/10.1115/1.3239900>
- Mueller, J. D., Hueckelheim, J., & Mykhaskiv, O. (2018). *STAMPS: A finite-volume solver framework for adjoint codes derived with source-transformation AD.* 2018 Multidisciplinary Analysis and Optimization Conference. American Institute of Aeronautics and Astronautics. <https://doi.org/doi:10.2514/6.2018-2928>
- Murman, E. M., & Cole, J. D. (1971). Calculation of plane steady transonic flow. *AIAA Journal*, 9, 114-121. <https://doi.org/10.2514/3.6131>
- Starken, H., & Schreiber, H. A. (1990). *Tests cases for computation of internal flows in aero engine components test case E/CA-4 low supersonic compressor cascade MCA.* AGARD-AR-275.
- Tweedt, D. L., Schreiber, H. A., & Starken, H. (1988). Experimental investigation of the performance of a supersonic compressor cascade. *ASME Journal of Turbomachinery*, 110(4), 456–466. <https://doi.org/10.1115/1.3262219>
- Wu, C. H. (1952). A general theory of three-dimensional flow in subsonic and supersonic turbomachines of axial, radial, and Mixed-Flow types. *Transactions of the American Society of Mechanical Engineers*, 74(8), 1363–1380. <https://doi.org/10.1115/1.4016114R>.